Dorais, M., Buchs D.M. Mineralogical characterization of rejuvenated magmatism at Burton Guyot, Louisville Seamount Trail, Contributions to Mineralogy and Petrology, v. 174 (66), doi.org/10.1007/s00410-019-1604-4, 2019.

MINERALOGICAL CHARACTERIZATION OF REJUVENATED MAGMATISM AT BURTON GUYOT, LOUISVILLE SEAMOUNT TRAIL

Michael J. Dorais
Department of Geological Sciences
Brigham Young University
Provo, Utah 84602
dorais@byu.edu

David M. Buchs
School of Earth and Ocean Sciences
Cardiff University
Cardiff, CF10 3AT UK
buchsd@cardiff.ac.uk

ABSTRACT

Volcaniclastic sequences drilled during IODP Expedition 330 on top of Burton Guyot preserve a unique record of rejuvenated magmatic activity along the Louisville Seamount trail. Geochemical analysis of clinopyroxenes in primary volcaniclastic deposits of this rejuvenated phase allows the reconstruction of magmatic evolution from the shield to post-erosional phases of a Louisville seamount, and to compare this evolution to that of Hawaiian volcanoes. Our results reveal the occurrence of three main types of clinopyroxenes in the rejuvenated volcaniclastic deposits at Burton Guyot, with a Na (and Al)-poor phenocrystic clinopyroxene and two types of Na-rich clinopyroxenes from disaggregated ultramafic xenoliths. The rejuvenated Na-poor phenocrysts have the same compositional range as clinopyroxenes associated with the shield stage of the volcano, indicating an overlap in shield and rejuvenated magma compositions. The dominant type of Na-rich clinopyroxene (Type 1) is very similar to clinopyroxenes in Hawaiian pyroxenitic xenoliths thought to represent high pressure cumulates. Their relatively low Mg/(Mg+Fe), Cr, and Sc contents, similar trace element abundances and high Al(vi):Al(iv) to Hawaiian cumulates indicates that they too are cumulates. This contrasts with lower Al(vi):Al(iv) of the Na-poor phenocrysts that crystallized between 6-7 kbars and 1150 – 1200 ºC. Type 2 clinopyroxenes are Mg-rich, and have major and trace element compositions very similar to clinopyroxenes in Hawaiian peridotites. These clinopyroxenes are interpreted as fragments of mantle xenoliths. They show intermediate amounts of incompatible element depletion, between more enriched Hawaiian peridotites and strongly depleted abyssal peridotites. Some grains exhibit the effects of mantle metasomatism, having spoon-shaped, chondrite-normalized REE patterns like those of Hawaiian peridotite xenoliths. The occurrence of disaggregated pyroxenitic cumulates and metasomatized mantle xenoliths in rejuvenated magmas of both Burton Guyot and Hawaiian islands suggests that the plumbing system of these volcanic systems share significant similarities. However, consistent with previous geochemical studies of the Louisville seamounts, geochemical consistency of shield and rejuvenated clinopyroxenes at Burton Guyot show that this volcano experienced similar alkaline magmatism from shield to rejuvenated stages. This is an important difference with the evolution of Hawaiian volcanoes that includes a dominantly tholeiitic shield stages and alkaline post-shield and rejuvenated stages, which suggests that the model of Hawaiian island formation may not be fully applicable to Louisville seamounts.

INTRODUCTION

The Louisville Seamount Trail (LST) is a chain of guyots and large volcanic seamounts that extends for approximately 4300 km across the Pacific Plate in the South Pacific Ocean (Figure 1) and forms the second longest seamount chains on Earth following the Hawaiian-Emperor Seamount Chain. The Louisville seamounts show an along-chain age progression, ranging from ~80 Ma for the Osbourn Guyot located at the northwestern end of the chain close to the Tonga Trench, to a ~1 Ma unnamed seamount at 50º26.4S, 139º10.0W at the southeastern end of the trail (Lonsdale, 1988; Koppers et al., 2011; 2012a). Similar to the Hawaiian-Emperor Seamount Chain, the LST is thought to have resulted from the Pacific Plate moving over a long-lived mantle hot spot. Also similar to the Hawaii-Emperor Seamount Chain, the LST shows a distinct bend at 169ºW (~50 Ma), which is thought to reflect a combination of changes in plate motion and mantle dynamics (Koppers et al., 2011; 2012b; Konrad et al., 2018). Because of its several similarities to the Hawaiian-Emperor Seamount Chain, better understanding the magmatic and volcanic evolution of the LST is significant to our understanding of intraplate oceanic volcanism on a fast-moving plate setting (i.e., like the Pacific Ocean in the Mesozoic). In particular, it remains critical to determine whether the magmatic evolution of the LST volcanoes undergo comparable evolutionary stages to Hawaiian-Emperor Seamount volcanoes that are commonly considered as an archetypal example of hotspot volcanism producing large volcanoes in the Pacific Ocean. Hawaiian volcanoes experience four sequential stages as the lithosphere approaches, moves over, and proceeds past an underlying mantle hot spot (Clague, 1987; Clague and Sherrod, 2014). These include a pre-shield stage with infrequent, small volume submarine eruptions of alkalic basalts, a shield stage with eruptions of frequent, large volumes of tholeiiic basalt, a post-shield stage where magmatism reverts to small volumes of alkalic basalt, and finally a strongly alkaline, rejuvenated stage that generally takes place following a magmatic hiatus of up to 2 m.y.

We provide herein new constraints on the late magmatic evolution of Burton Guyot that formed ca. 64 Ma along the LST (Koppers et al., 2012a; Heaton and Koppers, 2019), using fresh clinopyroxenes from primary volcaniclastic deposits that are associated with post-erosional rejuvenated magmatism of the seamount (Buchs et al., 2018). Our samples were retrieved by coring of the flat summit of the guyot during IODP Expedition 330 along the LST (Koppers et al., 2012a), and offer a valuable insight into the latest, rejuvenated magmatic phase of this volcano. Consistent with previous whole-rock and clinopyroxene geochemical results from the LST (Beier et al., 2011; Nicholls et al., 2014; Vanderkluysen,et al., 2014; Dorais, 2015), our data suggest limited geochemical changes from pre-erosional “shield” to post-erosional rejuvenated magmatism at Burton Guyot. We also recognize and characterize clinopyroxene xenocrysts in the rejuvenated units, which we suggest are from disaggregated ultramafic xenoliths, and provide a new insight into the magma plumbing system of a Louisville seamount.

GEOLOGIC SETTING

The studied samples were retrieved from Site U1376 of IODP Expedition 330 that is located close to the center of the summit platform of Burton Guyot and cross-cuts the southern side of a small conical feature that appears to have developed after formation of the flat summit (Figure 2). Although 5 Louisville seamounts were drilled during Expedition 330 (Koppers et al., 2012a), we focus on the Burton Guyot because it displays the strongest evidence for rejuvenated magmatism and includes disaggregated xenoliths. The conical feature on top of the guyot is considered here to be the volcanic edifice for rejuvenated volcanism on the basis of consistent petrographic, lithostratigraphic and petrological observations, as presented below.

Stratigraphic constraints for a rejuvenated stage at Burton Guyot

The summit of Burton Guyot was drilled down to 180 meters below sea level (mbsl) at Site U1376 of IODP Expedition 330, with an overall core recovery of 75% (Koppers et al., 2012a). Three main lithostratigraphic units were defined in this coring interval (Units I to III), which include clinopyroxene-bearing volcanic, volcaniclastic and sedimentary deposits that record transition from the shield to post-erosional stages (Koppers et al., 2012a; Buchs et al., 2018; this study).

The volcanic basement at Site U1376 on Burton Guyot corresponds to Unit III that was drilled from approximately 42 to 180 mbsf (Figure 3). This unit is composed of vesicular hyaloclastites with lava flows and subordinate crosscutting intrusive sheets (Koppers et al., 2012a). The unit above 57 mbsf includes rare, distinctive polymictic breccias and pillow lavas. The breccias include rare red-oxidized subrounded to rounded basalt clasts that suggest the occurrence of an emergent volcano during emplacement of the pillow lavas. Interbedded hyaloclastites and lava flows in the lower part of Site U1376 define a sequence that is best accounted for by submarine fragmentation of lava flows in lava-fed deltas and/or submarine slopes surrounding an emergent volcano (Buchs et al., 2018). Similar to other Louisville seamounts, degassing of the glass in the volcanic basement in the uppermost Burton Guyot at Site U1376 suggests shallow, albeit poorly constrained (~10–400 m), depth of eruption (Nichols et al., 2014) that is consistent with subaerial eruption followed by lava fragmentation in a shallow-marine environment. These observations and other stratigraphic relationships presented below suggest that Unit III was emplaced during the shield volcanic stage of Burton Guyot.

Post-shield volcaniclastic and sedimentary rocks overlying Unit III were divided into Units I and II based on their contrasted lithological characteristics (Figure 3; Koppers et al., 2012a). Unit II extends from 21.45 mbsf to the volcanic basement at 41.93 mbsf. This unit is predominantly composed of coralline algal boundstone to rudstone (Subunit IIA) associated with construction of a ~15 m-thick coralline algal framework on top of the seamount (Koppers et al. 2012a). The base of the algal boundstone to rudstone grades to a shallow-marine volcaniclastic conglomerate (Subunit IIB) that rests upon the volcanic basement along a major erosional unconformity similar to those seen on top of the basement at other drilled Louisville seamounts (Buchs et al., 2018). The conglomerate is rich in shallow-marine bioclasts and includes remarkable examples of micropeloidal cement (Buchs et al., 2018). These observations clearly document sedimentation in a high-energy, beach or shallow platform environment. The coastal/beach conglomerate at the base of the algal boundstone in Subunit IIB, erosional surfaces on top of the basement (boundary between units III and IIB), and absence of intrusive sheets in Units I and II (but their occurrence in underlying Unit III) suggest that Unit II emplaced after/during wave planation and subsidence of Burton oceanic island (Buchs et al., 2018).

Unit I that is the main focus of this study and most likely correlates to a rejuvenated volcanic cone on top of the summit platform of the guyot (Figure 2) occurs on top of the algal boundstone to rudstone of Unit II (Figure 3). Although the contact between Units I and II was not retrieved during coring (Koppers et al., 2012a), lithological changes from Units II to I show that Unit I deposited in a deeper marine environment. Notably, Subunits ID and IA at the base and the top of Unit I, respectively, include several polymictic volcaniclastic turbidites and bioturbated fine tuffaceous deposits, with several cm-thick interbedded ferromanganese crusts in Subunit IA (Koppers et al., 2012a; Buchs et al., 2018). These marine deposits encompass Subunits IB and IC that are mostly composed of monomictic lithic to vitric lapilli tuff with common hyperconcentrated flow structures and several erosional unconformities. Similarly to Buchs et al. (2018), this facies is interpreted here as primary volcaniclastic deposit emplaced in a deeper marine environment after initial subsidence of the seamount (i.e., post-erosional, rejuvenated

submarine volcanic activity). The interpretation of this facies is further supported by its likely correlation to the *untruncated* conical structure on top of the guyot (Figure 2), and ~120–350 m depth of eruption constrained by volatile contents in fresh glass fragments of Subunit IC (Nichols et al., 2014).

The absolute timing of emplacement of the units drilled on Burton Guyot remains poorly constrained due to difficulties in obtaining geochronological data in altered volcaniclastic products of Units I and II and overall paucity of datable fossils in the sedimentary deposits. Igneous rocks in the volcanic basement (Unit III) have very consistent ca. 64-63 Ma ages of crystallization (Koppers et al., 2012b; Heaton and Koppers, 2019). Late Oligocene-early Miocene depositional ages are suggested for minor chalk deposits associated with ferromanganese crusts in Subunit IA based on shipboard nannofossil observations (Koppers et al., 2012a). Based on these data it is not possible to determine the duration of the magmatic gap between the end of shield volcanism recorded in Unit III of the volcanic basement and rejuvenated (submarine) volcanism recorded in Subunits IB and IC. However, as summarized above, the occurrence of a main erosional surface between the volcaniclastic cover (Units I and II) and volcanic basement (Unit III), deposition of a relatively thick interval of algal framework in Unit II, and changes from shallow-marine to deep-marine environments between Unit II and the base of Unit I, support the occurrence of a magmatic gap between Unit III (shield stage) and Unit I (rejuvenated stage). Primary volcaniclastic products found in Subunits IB and IC offer therefore a unique opportunity to study post-erosional, rejuvenated volcanism of a Louisville seamount.

Petrography of rejuvenated volcaniclastic deposits

Clasts in rejuvenated breccias and tuffs of Subunits IB and IC range in size from 0.1 to 10 mm in diameter, and are mostly composed of basaltic fragments (Figure F11 of Koppers et al., 2012a). Some clasts contain clinopyroxene grains ranging in size between 1 and 7 mm in size, but many clinopyroxenes occur as individual grains scattered throughout the matrix of the breccias. Minor amounts of olivine and plagioclase are also present.

The rejuvenated, volcaniclastic deposits on Burton Guyot contain fragments of hornblende and biotite (Koppers et al. 2012a), implying eruption of rejuvenated magma more evolved than that represented by the more basic basement succession. Subunit IC also contains disaggregated ultramafic xenoliths as indicated by partly resorbed orthopyroxene xenocrysts in basalt clasts with clear reaction clinopyroroxene coronas in Subunit 1C (Figure F12 of Koppers et al. 2012a), suggesting that the rejuvenated stage magmas were strongly alkaline.

Geochemistry of the rejuvenated volcanic phase at Louisville seamounts

No lavas of rejuvenated compositions were drilled along the LST. The existence of a rejuvenated phase of magmatism at Louisville seamounts was previously recognized based on the composition of (i) whole rock samples recovered by dredging along the LST (Beier et al., 2011), and (ii) fresh glass in volcaniclastic deposits in Unit I at Site U1376 on Burton Guyot (Nichols et al., 2014). Beier et al. (2011) concluded (based on geochemical analysis and dating of dredged samples) that the youngest lavas on an individual guyot show the least enrichment in incompatible elements and suggested that the rejuvenated magmas likely resulted from re-melting of the previously depleted mantle that produced the shield stage volcanism. In contrast, Nichols et al. (2014) provided two analyses of glass sampled by drilling in the uppermost part of Burton Guyot, which are more enriched in K_2O and have higher La/Yb, Tb/Yb, and Nb/Zr values than shield lavas at this volcano. As explained above, lithostratigraphic criteria (Koppers et al., 2012a; Buchs et al., 2018) are consistent with the existence of a rejuvenated volcanic phase at

Site U1376 on Burton Guyot. However, it is less clear whether a similar phase exists at other Louisville Seamounts and could be identified based on geochemical constraints alone.

METHODS

Our study focused on the analysis of fresh pyroxenes preserved in rejuvenated volcaniclastic deposits in Unit I (Subunits IB and IC) at Site U1376 on Burton Guyot. Clinopyroxene and amphibole major element compositions were determined at Brigham Young University using a Cameca SX50 microprobe. Trace element concentrations in clinopyroxene were then determined at Memorial University of Newfoundland with an Element II ICP-MS. Analytical details are given in Dorais and Tubrett (2008). Additional clinopyroxene and amphibole analyses were obtained at GEOMAR and Christian Albrecht University following the methods of Buchs et al. (2015).

We compared the clinopyroxene compositions of the rejuvenated stage preserved in Unit I to those in the main, shield stage of the Burton Guyot preserved in Unit III to determine if Louisville rejuvenated magmas are compositionally distinct from the main shield stage as they are at Hawaii. We also compared Louisville rejuvenated clinopyroxene compositions to those in rejuvenated lavas of the Honolulu Volcanics of Oahu and from the submarine North Arch Volcanic Field to further evaluate the similarities/dissimilarities of Hawaiian and Louisville magmatic evolution. The North Arch lavas are thought to represent rejuvenated lavas that erupted along the flexural arch that surrounds the younger Hawaiian Islands (Frey et al., 2000). Hereafter, the clinopyroxenes from both the Honolulu Volcanics and the North Arch will simply be referred to as Hawaiian rejuvenated clinopyroxene.

RESULTS

Clinopyroxene Major Elements

Electron microprobe analyses of clinopyroxene from Site U1376A are presented in Table 1. Figure 4A plots clinopyroxene analyses from the rejuvenated stage compared to the clinopyroxene in the basement (i.e., shield stage). No differences are evident in this diagram. Figure 4B plots the Burton Guyot rejuvenated clinopyroxenes and clinopyroxene from Hawaiian rejuvenated lavas. Some of the Hawaiian clinopyroxenes are offset to higher Ca, either from higher Na contents (Morimoto et al., 1988), lower temperature (Lindsley, 1983) or both.

Figure 5 plots Na - Al-, Ti-, and Cr versus Mg/(Mg+Fe), Al(vi) versus Al(iv) and Ti versus Al cations per formula unit (cpfu). Figure 5A shows two distinct trends of clinopyroxene compositions. Clinopyroxene in the Burton Guyot basement rocks and clinopyroxenes grains in the primary volcaniclastic Unit I are similar in composition. The basement clinopyroxenes have moderate Na contents of ~ 0.03 cpfu over Mg/(Mg+Fe) range of 72 – 85 (Figure 5A), with the rejuvenated pyroxenes having the same Na contents at a given Mg/(Mg+Fe) but extending to slightly higher Mg/(Mg+Fe) values. There is some overlap of Hawaiian rejuvenated and Louisville clinopyroxenes, but most of the Hawaiian clinopyroxenes are richer in Na, reaching above 0.07 cpfu over a similar Mg/(Mg+Fe) span as the Burton Guyot basement clinopyroxenes.

In contrast, other Louisville clinopyroxenes from Subunit IC define a separate trend, being distinctly richer in Na than all basement and rejuvenated clinopyoxenes with values up to 0.16 cpfu at low Mg/(Mg+Fe). These clinopyroxenes are very similar in composition to clinopyroxene in pyroxenite xenoliths from Kaula Island, Hawaii (Presti, 1982; Bizimis et al., 2013) and Salt Lake Crater, Oahu (Sen, 1988; Sen et al., 1993; Bizimis et al., 2005; Keshav et al., 2007). Hence, we refer to these Na-rich Louisville clinopyroxenes as xenocrystic, having been derived from

disaggregated ultramafic xenoliths, and call them Type 1 clinopyroxenes. Other Hawaiian clinopyroxenes from peridotites on Oahu are also Na-rich, but have higher Mg/(Mg+Fe) than clinopyroxenes in Hawaiian pyroxenites. Notably, a minor subset of Na-rich Louisville pyroxenes is similar to clinopyroxenes from Hawaiian peridotites and have 100Mg/(Mg+Fe) values as high as 92. We refer to these as Type 2 clinopyroxenes. Abyssal peridotite clinopyroxene compositions also have high Mg/(Mg+Fe) values but with lower Na concentrations (Johnson and Dick, 1992).

The majority of basement and rejuvenated Louisville clinopyroxenes show much overlap in the Al (cpfu) versus Mg/(Mg+Fe) diagram (Figure 5B) with Al contents ranging from 0.1 to 0.3 cpfu. Hawaiian rejuvenated clinopyroxenes have similar Mg/(Mg+Fe) values but some plot at slightly higher Al contents at Mg/(Mg+Fe) values of less than 80. Most of the Louisville Type 1 clinopyroxene is richer in Al than rejuvenated and basement clinopyroxene and is very similar to clinopyroxene from Hawaiian pyroxenite xenoliths. Clinopyroxene from Hawaiian peridotites and abyssal peridototes are moderately rich in Al as are the Type 2 Louisville pyroxenes at high Mg/(Mg+Fe).

The Ti versus Mg/(Mg+Fe) diagram (Figure 5C) shows two trends that increasingly diverge at lower Mg/(Mg+Fe) values. With decreasing Mg/(Mg+Fe), the high Ti trend consists of overlapping compositions of Louisville basement and rejuvenated clinopyroxene from both Louisville and Hawaii. In contrast, the Na-rich clinopyroxene from Kaula Island, Salt Lake Crater and Type 1 Louisville have lower Ti concentrations. Clinopyroxene from spinel peridotites from Oahu, the abyssal peridoties, and the Type 2 Louisville clinopyroxenes are the most Mg/(Mg+Fe)-rich and have low Ti concentrations.

As in previous diagrams, the Louisville basement and rejuvenated clinopyroxenes show considerable overlap in the Cr versus Mg/(Mg+Fe) diagram (Figure 5D) and are similar to Hawaiian rejuvenated clinopyroxene. However, some rejuvenated clinopyroxenes from Burton Guyot have higher Mg/(Mg+Fe) and Cr contents than the Louisville basement clinopyroxenes. The Type 1 Louisville clinopyroxenes have low Cr concentrations regardless of the Mg/(Mg+Fe) value. In contrast, the Type 2 Louisville Na-rich clinopyroxenes are both Cr- and Mg-rich, plotting with the clinopyroxene from abyssal pyroxenes and the Oahu peridotites.

Separation of the xenolithic and phenocrystic clinopyroxenes is also displayed in the Al(vi) versus Al(iv) diagram (Figures 5E). The Louisville rejuvenated and basement clinopyroxenes show good correspondence, plotting low Al(vi):Al(iv) as do Hawaiian rejuvenated clinopyroxene. Low Al(vi):Al(iv) values are indicative of low pressures of crystallization (Wass, 1979). In contrast, the Na-rich clinpyroxenes from Kaula Island, Salt Lake Crater and other Oahu locations clinopyroxenes have high Al(vi):Al(iv) ratios. The Type 1 and Type 2 xenolithic clinopyroxenes from Louisville also plot at high Al(vi):Al(iv) ratios, reflecting relatively high pressures of crystallization (Wass, 1979).

Finally, all Louisville phenocrystic clinopyroxene from both the basement and the rejuvenated phase, as well as the Hawaiian rejuvenated samples, define a trend that is distinct from all the xenolithic pyroxenes in the Ti versus Al diagram (Figure 5F). Type 2 Louisville clinopyroxenes and those from Hawaiian peridotites plot with the abyssal clinopyroxenes; the Type 1 Louisville clinopyroxene plots with the clinopyroxene from Hawaiian pyroxenites.

Based on these electron microprobe analyses of Burton Guyot clinopyroxenes, we classify the clinopyroxenes in three groups: 1) phenocrysts of the shield and post-erosional/rejuvenated volcanic phases. Based on clinopyroxene major element chemistry, there is no distinction between the volcanic basement in Unit III and volcaniclastic cover in Subunits IB and IC. Other than being slightly richer in Na, Hawaiian rejuvenated clinopyroxenes are similar to Louisville phenocrysts; 2) Type 1 Louisville clinopyroxenes, which are restricted to the rejuvenated volcanic

phase. These pyroxenes are very similar to clinopyroxenes in Hawaiian pyroxenites from Kaula Island and Salt Lake Crater on Oahu; and 3) Type 2 Louisville clinopyroxenes, which are stratigraphically associated with Type 1 clinopyroxenes. Type 2 Louisville clinopyroxenes are similar to clinopyroxenes from Hawaiian and abyssal peridotites.

Clinopyroxene Trace Elements

Trace element analyses of Burton Guyot clinopyroxenes are presented in Table 2. Figure 6A plots chondrite-normalized REE patterns for Burton Guyot clinopyroxenes. All these grains have Mg# between 79 and 81, hence they represent clinopyroxenes that crystallized from magmas of similar degrees of differentiation. The REE concentrations in grains from the basement show a range in REE concentrations. Clinopyroxene from core samples 1376A-8R5 58/61 and 1376A-13R4 8/10 in the upper part of the volcanic basement show moderate REE abundances (Table 2), with La_N ranges from 72.6 to 143.6 and $(La/Yb)_N$ from 4.46 to 8.9. In contrast, the deepest sample analyzed from the basement, 1376A-23R6 32/35, is REE rich, with La_N ranging from 199.9 to 261.0 and $(La/Yb)_N$ ranging from 11.4 to 12.6. Rejuvenated clinopyroxene has intermediate REE abundances, overlapping the values displayed by the basement clinopyroxene. La_N ranges between 108.6 to 254.3 and $(La/Yb)_N$ is also intermediate, from 6.65 to 10.54.

Chondrite-normalized REE patterns for the Type 1 clinopyroxenes are also plotted in Figure 6A. They display similar LREE abundances to Louisville phenocrysts, but the HREE are lower with Lu_N values between 2.1 and 0.78 compared to phenocryst values between 8.2 and 2.98. Figure 6B compares these Louisville clinopyroxenes to clinopyroxene in Kaula Island and Salt Lake Crater pyroxenites. Salt Lake Crater clinopyroxenes (Bizimis et al., 2005) have the same convex upward patterns but are slightly richer in LREE than Louisville xenolithic clinopyroxenes. Kaula Island clinopyroxenes are more HREE-rich with flatter patterns (Bizimis et al., 2013).

Figure 6C plots clinopyroxene patterns from spinel peridotites from Kaau, Pali, and Kalhi on Oahu (Sen et al., 1993). Also shown are analyses of clinopyroxene from depleted mantle (Johnson and Dick, 1992; Neumann et al., 2005) that show strong LREE depletions. Some of the Hawaiian clinopyroxenes show similar depleted patterns to the N-MORB field. Others have similar MREE to HREE patterns, but display a distinct spoon-shaped LREE pattern that Sen et al. (1993) attributed to metasomatic enrichment of the LREE. Two analyses of the Na-rich, Type 2 clinopyroxenes have the same spoon-shaped patterns as metasomatized clinopyroxene from Hawaiian peridotites (Sen et al., 1993).

Louisville clinopyroxene Y versus Zr, Sr versus Zr/Y and Sc versus Zr/Y are presented in Figure 7. Louisville rejuvenated and basement clinopyroxenes define coherent trends with the basement clinopyroxenes showing the widest range in compositions, e.g., Zr/Y values range from 1.60 to 4.77. Rejuvenated clinopyroxenes plot at intermediate values along the trends, with rejuvenated clinopyroxene with intermediate Zr/Y values of 2.5 to 3.6. The Type 1 clinopyroxenes are distinct from the phenocrysts, particularly in the Sc versus Zr/Y diagram (Figure 7C) where their very low Sc concentrations are evident. The Type 2 clinopyroxenes overlap the compositional range of clinopyroxene from pyroxenitic xenoliths from Salt Lake Crater, Oahu.

Amphibole Compositions

Amphibole crystals are present as sparse, individual crystals in the volcaniclastic deposits. The composition of the grains exhibits a considerable range, extending from tschermakite to

actinolitic-hornblende (Figure 8). The tschermakite is relatively rich in Cr, containing up to 0.68 wt.% Cr_2O_3 (Table 3). With increasing Si contents, the Cr_2O_3 contents decline to below detection limits. Also plotted in the figure are amphibole analyses that rim clinopyroxene-bearing xenoliths from Mauna Kea, Hawaii (Pickard, 2008). These Hawaiian amphiboles appear to form metasomatic, reaction rims on the outer margins of some xenoliths, and are similar in composition to the tschermakite at Burton Guyot.

DISCUSSION

Nature of the Louisville Rejuvenated Magmas

One of the major goals of IODP Expedition 330 was to determine if the Louisville Seamount Chain volcanoes shows a similar magmatic evolutionary history to the Hawaiian Emperor Seamount Trail. Although Beier et al. (2011) suggest based on the composition of dredged samples that rejuvenated magmatism is more depleted than the main, shield-building stage in Louisville volcanoes, Nicholls et al. (2014) show based on the analysis of two glass samples collected during IODP Expedition 330 that the uppermost portion of the Burton Guyot (including the studied volcaniclastic deposits) has a more alkaline composition than the pre-erosional basement of this seamount. New lithostratigraphic observations (Buchs et al., 2018; this study) and occurrence of a conical feature on the summit of the seamount (Fig. 2) demonstrate that a rejuvenated volcanic phase exists at Burton Guyot. However, the composition of this phase and how it compares to the shield-building stage require further investigation.

In each of the clinopyroxene chemical diagrams, the Louisville basement and rejuvenated compositions completely overlap, not only for major elements (Figures 4 and 5) but for trace elements as well (Figures 6A and 7). The range in Zr/Y and Nb/Y values of Burton Guyot clinopyroxene is especially pertinent in deciphering the relationship between shield and rejuvenated magmas. In basaltic systems, both Zr and Nb are incompatible elements of similar behavior during mantle melting. Yttrium is less incompatible, hence ratios of Nb/Y and Zr/Y vary as a function of the amount of partial melting (Pearce and Norry, 1979; Fitton et al., 1997; Baksi, 2001). Because zircon is not saturated in these basaltic magmas, crystal fractionation does not change these ratios. Additionally, the very narrow range of Mg# of the analyzed clinopyroxenes also indicates limited fractionation. The wide range of Zr/Y values of clinopyroxene in the basement rocks (Figure 7) suggests that the pyroxenes crystallized from basalts generated by variable amounts of partial melting. Rejuvenated clinopyroxene has Zr/Y values that are intermediate to that of the basement clinopyroxenes, suggesting that they crystallized from basalts formed from intermediate amounts of partial melting relative to basalts in the basement. Thus, our limited clinopyroxene data give no indication that the rejuvenated magmas were either more or less depleted than the main, shield stage magmas. Additional research may provide a broader spectrum of mineral compositions that may verify the hint of more enriched, rejuvenated compositions determined by Nicholls et al. (2014).

Apparent similarity of rejuvenated and shield magmatism at Burton Guyot is further emphasized in the Nb/Y versus Zr/Y diagram (Figure 9), in which liquid compositions were calculated using the cpx compositions and cpx/basalt partition coefficients listed in Dorais (2015). Although these coefficients were determined empirically, they were specifically calibrated for the LST magmatic system at several seamounts. Therefore, these coefficients allow us to provide an additional, albeit possibly semi-quantitative assessment of melt variability at Burton Guyot based on clinopyroxene composition. Fitton et al. (1997) defined an array for Icelandic lavas to determine the relative influence of the Icelandic plume along the North Atlantic MOR, but the diagram can be used to provide additional constraints on ocean island basalts globally. Figure 9 shows whole-rock analyses of Louisville rocks (Fitton, personal communication, 2014) and glass analyses of

Nicholls et al. (2014), including the two analyses of rejuvenated glass mentioned above. Our calculated compositions of liquids in Burton basement plot along the Iceland array over a range of Nb/Y and Zr/Y values, indicating variable amounts of partial melting produced the liquids from which the clinopyroxenes crystallized. Of specific interest is the range of calculated liquid compositions of the rejuvenated lavas compared to the shield stage liquids. Recalculated rejuvenated liquids plot with the glass and whole-rock analyses and within the array defined by basement clinopyroxenes. This observation suggests that the rejuvenated magmas from which these clinopyroxenes crystallized, unlike Hawaii where rejuvenated magmas are more alkalic than the alkaline post-shield lavas, are not significantly distinct from the shield stage magmas at Burton Guyot.

Minor variability and discrepancy between the composition of whole rock samples and Cpx-derived liquids at Burton Guyot could be related to errors in our liquid-Cpx Kds. Alternatively, many of these clinopyroxene phenocrysts could be anticrysts, having crystallized from earlier melts in the Louisville system. Melt inclusions in phenocrysts commonly display a larger range in compositions than whole-rock compositions, reflecting a more complete record of the range of melts that mixed to produce the final bulk-rock composition (Kent, 2008). Likewise, the Burton clinopyroxenes could have crystallized from a sequence of magmas derived by variable amounts of partial melting, which, upon mixing, yielded a limited range of bulk-rock compositions. The final magmas may have carried a cargo of anticrystic crystals.

How then do we reconcile the apparent contradiction between Beier et al. (2011) who concluded that the Louisville rejuvenated magmas were depleted compared to the magmas of the shield-building stage, with the opposite conclusion reached by Nicholls et al. (2014)? In the uppermost basement of Burton Guyot, clinopyroxene data suggests that the degree of partial melting became progressively higher during the main volcanic phase of the seamount/oceanic island (Dorais, 2015; this study). Our rejuvenated samples suggest a return to lower amounts of partial melting, but not as low as the deepest basement sample. It is conceivable that the amount of partial melting varied throughout the magmatic history of the Burton Guyot, not just for basement magmas, but for rejuvenated magmas as well, and that the sampling of the rejuvenated phase of each study, including ours, was not sufficiently representative of the breadth of magma compositions. This is not surprising considering the limited sampling available via deep sea dredging and drilling, and that the provenance of fresh volcanic glass from the rejuvenated phase at Burton Guyot (Nichols et al., 2014) does not overlap with that of clinopyroxenes analyzed in this study. Taken together, all three studies suggest variable amounts of partial melting produced the rejuvenated magmas in the LST.

Origin of Xenolithic Clinopyroxenes

The high Na, Al, and low Ti contents of the Louisville xenolithic clinopyroxenes indicate that these grains did not crystalized in equilibrium with their carrier melts. Instead these clinopyroxenes are very similar to those in Hawaiian xenoliths in all elements, including having high Al(vi) versus Al(iv) values indicative of relatively high-pressure crystallization. These Louisville clinopyroxenes could therefore have been derived from abyssal peridotites or disaggregated cumulates from alkaline melts that erupted along the LST.

Several factors suggest that most of the Louisville xenolithic clinopyroxenes are cumulates. First, the clinopyroxene is are very similar to those of Kaula Island and Salt Lake Crater pyroxenites, both in major and trace elements, that have been interpreted to be cumulates (Frey, 1980; Sen, 1988; Keshav and Sen, 2001;; Bizimis et al., 2005, 2013; Keshav et al., 2007; Sen et al., 2011). This interpretation is based on the lower Mg/(Mg+Fe), Cr, and Sc concentrations of clinopyroxene, the differences of chondrite-normalized REE patterns, and the

high Na and Al values compared to abyssal clinopyroxenes, Additionally, the similarity of isotopic characteristics of the xenoliths with the rejuvenated, Honolulu Volcanics suggests a consanguineous relationship that is also distinct from abyssal peridotites (Bizimis et al., 2005).

The identity of the Type 1 clinopyroxenes is further explored in Figure 10. These figures show two trends. The first is defined by clinopyroxene in abyssal and Hawaiian peridotites, forming subhorizontal trends at high Mg#. The second set defines negative trends that start at Mg# of ~86 and extends down to Mg# of ~70. These negative trends have been interpreted by Bizimis et al. (2013) to indicate crystal fractionation. They modelled clinopyroxene compositions from Kaula Island and Salt Lake Crater being in equilibrium with a fractionating melt whose parent composition is similar to the Honolulu Volcanics and the Kaula Island nephelinites. The lines with tick marks on the figures are their calculated compositions, ranging from 0.1% to 70% fractionation. Their model reproduces the observed clinopyroxene data well. Louisville Na-rich clinopyroxenes show the same negative correlations between Na_2O, Al_2O_3, Zr, Sm, and Ti versus Mg/(Mg+Fe) as the Kaula and Salt Lake Crater clinopyroxenes (Figure 10), suggesting that they too represent cumulates. Unlike the Type 2 clinopyroxenes and those from Salt Lake Crater peridotites that show spoon-shaped LREE patterns indicative of metasomatism (Sen et al., 1993), no upturn of the LREE patterns are evident for Type 1 clinopyroxenes.

Type 2 clinopyroxenes from Burton Guyot are Mg rich, with 100Mg/(Mg+Fe) values of ~90-92, plotting along the trends defined by clinopyroxene from abyssal and Hawaiian peridotites (Figure 10), suggesting that these Louisville clinopyroxenes are from disaggregated mantle xenoliths. They plot at intermediate values between the Salt Lake Crater and abyssal clinopyroxeens indicating moderate amounts of depletion. An origin as disaggregated mantle xenoliths is also consistent with co-occurrence of Type 2 clinopyroxenes with orthopyroxenes in rejuvenated volcaniclastic deposits in the summit of Burton Guyot (Koppers et al., 2012a).

Pressures and Temperatures of Equilibration

Pressures and temperatures of crystallization for Louisville clinopyroxene phenocrysts were calculated using the thermobarometer of Putirka et al. (2003). We used the average composition of shield glass analyses of Nicholls et al. (2014) to represent liquid compositions and the average compositions of four different clinopyroxene phenocrysts. The calculations meet the criteria for equilibrium of Putirka et al. (2003), yielding pressures averaging 7 kbars and temperatures of 1190 ^oC, plotting along the peridotite solidus (Figure 11; Hirschmann, 2000). These P-T conditions are comparable to those of clinopyroxene in other alkalic basalts (e.g., Nimis, 1999; Nikogosian et al., 2002; Ashchepkov et al., 2017), and are reproduced by MELTS using the average glass composition with 2 wt.% H_2O (Gualda et al., 2012).

Barometric studies of Hawaiian ultramafic xenoliths found in rejuvenated lavas indicate relatively high pressures of equilibration. Keshav et al. (2007) interpreted the Salt Lake Crater pyroxenites as cumulates based on liquidus phase relations in the CaO-MgO-Al_2O_3-SiO_2 system and suggested that the cumulates crystallized at pressures between 30 and 50 kbars. Pyroxenites from Salt Lake Crater studied by Bizimis et al. (2005) yield pressures between 11 and 34 kbars, Kaula Island pyroxenites show a smaller pressure range between 8 and 20 kbars (Bizimis et al., 2013). All these studies concluded that the pyroxenites resulted from high pressure crystal fractionation of rejuvenated-type magmas in the oceanic mantle. We lack the full mineral assemblage of their cumulates that would allow thermobarometic calculations, but we note that our clinopyroxenes have the same Na, Ti, and Al compositions and plot at the same high Al(iv):Al(vi) values indicative of similar high pressures of crystallization (Figure 5E).

Pressures and temperatures determined using single crystal pyroxene thermobarometry can be imprecise (Tartarotti et al., 2002). The Nimis and Taylor (2000) thermometer requires clinopyroxene to be in equilibrium with orthopyroxene, a condition not met for alkaline basalts, otherwise it yields temperatures that are too low (Nimis, personal communication, 2018). Our calculated temperatures for Type 1 clinopyroxenes range from 1050 to 1100° C. Likewise, the anhydrous formulation of the Nimis and Ulmer (1998) geobarometer for basalts is temperature independent, but underestimates pressure for hydrous systems by about 1 kbar per 1% H_2O in the melt. Our pressures average is ~ 17 kbars (Figure 11). Notwithstanding the large errors associated with single crystal thermobarometry, our calculations are similar to those determined for spinel pyroxenites from Hawaii, indicating that the Type 1 clinopyroxenes also crystallized at relatively high pressure, considerably higher than the phenocrysts that crystallized between 6-8 kbars.

The thermobarometer of Ridolfi and Renzulli (2012) was used to calculate P and T for Burton Guyot amphiboles. The Cr-rich tschermakite yields the highest temperatures of ~ 1020 °C at pressures of ~ 3.5 kbars. Owing to their high Cr contents (up to 0.68 wt. % Cr_2O_3), we interpret these amphibole grains as having formed in reaction with xenolithic clinopyroxene as the host magma differentiated enough to crystalize amphibole, similar to the Mauna Kea xenoliths (Pickard, 2008). Cr-poor amphibole phenocrysts (<0.05 wt. %) subsequently formed at progressively lower temperatures and pressures, having crystallized from Cr-depleted magmas that previously experienced considerable clinopyroxene fractionation. These amphiboles reflect an increasingly differentiated and more water-rich melt as rejuvenated magmas ascended and cooled.

CONCLUSIONS

The Burton Guyot of the Louisville Seamount trail exhibits similarities with volcanoes of the Hawaiian Emperor Seamount Chain, having a shield and rejuvenated stage. Three types of clinopyroxenes can be identified in deposits of the rejuvenated phase in Burton Guyot based on major and trace element contents: a phenocryst type and two types of clinopyroxene from disaggregated ultramafic xenoliths.

Phenocrystic clinopyroxenes of the rejuvenated phase are indistinguishable from clinopyroxenes of the shield phase in both major and trace element compositions. This indicates that, at Burton Guyot, the rejuvenated magma from which the clinopyroxenes crystallized was not more alkaline than the shield magmas. Clinopyroxenes from the Louisville rejuvenated magmas are similar to clinopyroxenes from the Hawaiian rejuvenated phase except the latter are slightly more Na-rich. These are significant results that suggest that the compositional range of the shield to rejuvenated stage magmas in Louisville seamounts is not as diverse as that documented at Hawaiian volcanoes during the same shield to post-erosional/rejuvenated volcanic interval. The apparent discrepancy between Beier et al. (2011) and Nicholls et al. (2014) that the rejuvenated magmas at Louisville seamounts were less and more enriched than the shield-phase magmas, respectively, can be resolved with variable extents of partial melting to produce magmas during both the shield and rejuvenated phases at Louisville seamounts, as suggested by our clinopyroxene results from Burton Guyot.

Like Hawaiian rejuvenated lavas, the primary volcaniclastic deposits in the summit of Burton Guyot carry disaggregated ultramafic xenoliths with Na-rich clinopyroxenes. At Site U1374 these clinopyroxene can be subdivided into Types 1 and 2 xenocrystic clinopyroxenes based on their major and trace element affinities. Type 1 clinoyproxenes are the more abundant xenocrystic pyroxenes, with Mg/(Mg+Fe)-, Cr-, and Sc-poor geochemical characteristics similar to those of clinopyroxenes from Hawaiian pyroxenites. Both Hawaiian and Louisville Type 1 clinopyroxenes

define fractionation trends in Na_2O, Al_2O_3, Zr, Sm, and Ti versus Mg# that support a cumulate origin. In addition, the Louisville grains have high Al(vi):Al(iv) values, similar to Hawaiian cumulates that crystallized between 12 to 20 kbars. Type 2 clinopyroxenes at Burton Guyot match the compositions of clinopyroxenes from Hawaiian peridotites and were likewise derived from abyssal peridotites. The composition of Type 2 clinopyroxenes suggest that Burton Guyot peridotites are moderately depleted, with compositions intermediate between strongly depleted abyssal peridotites and relatively enriched, Hawaiian peridotites. Metasomatic effects are suggested by LREE enrichment similar to that observed in metasomatized peridotite clinopyroxene at Hawaii. Finally, replacement of xenocrystic (Cr-rich) clinopyroxenes by amphiboles during crustal ascend and melt differentiation at Burton Guyot is suggested by association of these minerals in volcaniclastic deposits of the rejuvenated volcanic phase.

ACKNOWLEDGEMENTS

We are grateful to the captain and crew of the JOIDES Resolution in both the operation of the ship and the recovery of IODP 330 drill core. We also thank the highly professional IODP technical staff that made our time aboard ship very productive, Mike Garcia who provided thin sections of the Honolulu Volcanics, and Anthony Koppers and an anonymous reviewer for helpful comments on this manuscript. This research was funded by IODP post-expedition awards (USSP for M.J.D. and ANZIC for D.M.B.). This paper is dedicated to John J. Mahoney, a well-regarded member of Expedition 330.

REFERENCES

Anders, E., & Ebihara, M. (1992) Solar-system abundances of the elements. Geochimica et Cosmochimica Acta, 46, 2363-2380.

Ashchepkov, I.V., Ntaflos, T., Logvinova, A.M., Spetsius, Z.V, & Downes, H. (2017) Monomineral universal clinopyroxene and garnet barometers for peridotitic, eclogitic and basaltic systems. Geoscience Frontiers, 8, 775-795.

Baksi, A. (2001) Search for a deep-mantle component in mafic lavas using a Nd-Y-Zr plot. Canadian Journal of Earth Sciences, 38, 813-824.

Beier, C., Vanderkluysen, L., Regelous, M., Mahoney, J.J., & Garbe-Schönberg, D. (2011) Lithospheric control on geochemical composition along the Louisville Seamount Chain. Geochemistry, Geophysics and Geosystems, 12, Q0AM01, doi:10.1029/2011GC003690.

Bizimis, M., Sen, G., Salters, V.J.M., & Keshav, S. (2005) Hf-Nd-Sr isotope systematics of garnet pyroxenites from Salt Lake Crater, Oahu, Hawaii: Evidence for a depleted component in Hawaiian volcanism. Geochimica et Cosmochimica Acta, 69, 2629-2646.

Bizimiz, M., Salters, V.J.M., Garcia, M.O., & Norman, M.D. (2013) The composition and distribution of the rejuvenated component across the Hawaiian plume: Hf-Nd-Sr-Pb isotope systematics of Kaula lavas and pyroxenite xenoliths. Geochemistry, Geophysics, Geosystems, 14, doi: 10.1002/ggge.20250.

Buchs, D., Cukur, D., Masago, H., & Garbe-Schönberg, D. (2015) Sediment flow routing during formation of forearc basins: Constraints from integrated analysis of detrital pyroxenes and stratigraphy in the Kumano Basin, Japan. Earth and Planetary Science Letters, 414, 164-175.

Buchs, D.M., Williams, R., Sano, S., & Wright, V.P. (2018) Non-Hawaiian lithostratigraphy of Louisville seamounts and the formation of high-latitude oceanic islands and guyots. Journal of Volcanology and Geothermal Research, 356, 1-23.

Clague, D. A. (1987) Hawaiian alkaline volcanism. In: Fitton, J.G. and Upton, B.G. (ed.) Alkaline Igneous Rocks. Geological Society Special Publication No. 30, 227-252.

Clague, D.A., & Sherrod, D.R. (2014) Chapter 3: Growth and Degradation of Hawaiian Volcanoes. In: Characteristics of Hawaiian Volcanoes. Poland, M.P., Takahashi, T.J., Landowshi, C.M. (Editors), U.S. Geological Survey Professional Paper 1801, 97-146.

Dorais, M. J. (2015) Exploring the mineralogical heterogeneities of the Louisville Seamount Trail, Geochemistry. Geophysics, Geosystems, 16, 2884–2899, doi:10.1002/2015GC005917.

Dorais, M.J., and Tubrett, M., 2008. The identification of a subduction zone component in the Higganum dike, Central Atlantic Magmatic Province: A LA_ICPMS study of clinopyroxene with implications for flood basalt petrogenesis. Geochemistry, Geophysics, Geosystems, 9:Q10005. http:/doi.org/10.1029/2008GC002079.

Ducea, M., Sen, G., Eiler, J., & Fimbres, J. (2002) Melt depletion and subsequent metasomatism in the shallow mantle beneath Koolua volcano, Oahu (Hawaii). Geochemistry, Geophysics, Geosystems, 3 DOI: 10.1029/2001GC000184.

Fitton, J. G., Saunders, A.D., Norry, M.J., Hardarson, B.S., & Taylor, R.N. (1997) Thermal and chemical structure of the Iceland plume, Earth and Planetary Science Letters, 153, 197–208.

Frey, F.A. (1980) The origin of pyroxenite and garnet pyroxenites from Salt Lake Crater, Oahu, Hawaii: Trace element evidence. American Journal of Science, 280A, 427-449.

Frey, F.A., Clague, D., Mahoney, J.J., & Sinton, J.M. (2000) Volcanism at the edge of the Hawaiian plume: Petrogenesis of submarine alkali lavas from the North Arch volcanic field. Journal of Petrology, 41, 667-691.

Gualda G.A.R., Ghiorso M.S., Lemons R.V., & Carley T.L. (2012) Rhyolite-MELTS: A modified calibration of MELTS optimized for silica-rich, fluid-bearing magmatic systems. Journal of Petrology, 53, 875-890.

Heaton, D.E., and Koppers, A.A.P., 2019. High resolution 40Ar/39Ar geochronology of the Louisville Seamounts IODP expedition 330 drill sites: Implications for the duration of hotspot-related volcanism and age progression. Geochemistry, Geophysics, Geosystems, http: //doi/org/10.1029/2000GC000070.

Hirschmann, M.M. (2000) Mantle solidus: Experimental constraints and the effects of peridotite composition. Geochemistry, Geophysics, Geosystems, 1, 1042, doi:10:1029/2000/GC000070.

Johnson, K.T., & Dick, H.J.B. (1992) Open system melting and temporal and spatial variation of peridotite and basalt at the Atlantis II Fracture Zone. Journal of Geophysical Research, 97, 9219-9241.

Johnson, K.T., Dick, H.J.B., & Shimizu, N. (1990) Melting in the oceanic upper mantle: An ion microprobe study of diopsides in abyssal peridotites. Journal of Geophysical Research, 95, 2661-2678.

Kent, A.J.R. (2008) Melt inclusions in basaltic and related volcanic rocks. In: Minerals, Inclusions, and Volcanic Processes, Putirka, K.D., and Tepley, F.J.III (eds), Reviews in Mineralogy and Geochemistry, Vol. 69, 273-331.

Keshav, S., & Sen, G., 2001. Majoritic garnets in Hawaiian xenoliths: Preliminary results. Geophysical Research Letters, 28, 3509-3512.

Keshav, S., Sen, G., & Presnall, D.C. (2007) Garnet-bearing xenoliths from Salt Lake Crater, Oahu, Hawaii: High-pressure fractional crystallization in the oceanic mantle. Journal of Petrology, 48, 1681-1724.

Konrad, K., Koppers, A.A.P., Steinberger, R., Finlayson, V.A., Konter, J.G., & Jackson, M.G. (2018) On the relative motions of long-lived Pacific mantle plumes. Nature Communications, DOI: 10.1038/s41467-018-03277.

Koppers, A.A.P., Yamazaki, T., Geldmacher, J., Gee, J.S., 2010. Louisville Seamount Trail: Implications for geodynamic mantle flow models and the geochemical evolution of primary hotspots. Integrated Ocean Drilling Program Scientific Prospectus. http://doi.org/10.2204/iodp.sp.330.2010.

Koppers, A.A.P., Gowen, M.D., Colwell, L.E., Gee, J.S., Lonsdale, P.F., Mahoney, J.J., & Duncan, R.A. (2011) New $^{40}Ar/^{39}Ar$ age progression for the Louisville hot spot train and implications for inter-hot spot motion. Geochemistry, Geophysics, and Geosystems 12, Q0AM02, doi:10.1029/2011GC003804.

Koppers, A.P., Yamazaki, T., Geldmacher, J, Anderson, L., Beier, C., Buchs, D.M., Chen, L., Cohen, B.E., Deschamps, F., Dorais, M.J., Ebuna, D.R,. Ehmann, S., Fitton, J.G ., Fulton, P.M., Ganbat, E., Gee, J.S, Hamelin, C., Hanyu, T., Hoshi, H., Kalnins, L., Kell, J., Machidi, S., Mahoney, J.J., Moriya, K., Nichols, A.R.L., Pressling, N.J., Rausch, S., Sano, S., Sylvan, J.B., & Williams, R. (2012a) Proceedings of the Integrated Ocean Drilling Program Volume 330. http://publications.iodp.org/proceedings/330/330toc.htm.

Koppers, A.A.P., Yamazaki, T., Geldmacher, J., Gee, J.S., Pressling, N., Hoshi H., Anderson, L., Beier, C., Buchs, D.M., Chen, L., Cohen, B.E., Deschamps, F., Dorais, M.J., Ebuna, D.R,. Ehmann, S., Fitton, J.G., Fulton, P.M., Ganbat, E., Hamelin, C., Hanyu, T., Kalnins, L., Kell, J., Machidi, S., Mahoney, J.J., Moriya, K., Nichols, A.R.L., Rausch, S., Sano, S., Sylvan, J.B., & Williams, R. (2012b) Limited latitudinal mantle plume motion for the Louisville hotspot. Nature Geoscience, 5, 911-917, (doi:10.1038.NGEO1638).

Lindsley, D.H. (1983) Pyroxene thermometry. American Mineralogist, 68, 477–49

Lonsdale, P. (1988). Geography and history of the Louisville hotspot chain in the southwest Pacific. Journal of Geophysical Research: Solid Earth, 93, 3078-3104.

Morimoto, N., Fabreis, J., Ferguson, A.K., Ginzburg, I.V., Ross, M., Siefert, F.A., Zussman, J., Aoki, K., & Gottardi, G. (1988) Nomenclature of pyroxenes. American Mineralogist, 73, 1123-1133.

Neumann, E-R., Vannucci, R., & Tiepolo, M. (2005) N-MORB crust beneath Fuerteventura in the easternmost part of the Canary Island: evidence from gabbroic xenoliths. Contributions to Mineralogy and Petrology, 150, 156-173.

Nichols, A.R.L., Beier, C., Brandl, P.A., Buchs, D.M., & Krumm, S.H. (2014) Geochemistry of volcanic glasses from the Louisville Seamount Trail (IODP Expedition 330): Implications for eruption environments and mantle melting. Geochemistry, Geophysics and Geosystems, 15, 1718-1738; doi:10.1002/2013GC005086.

Nikogosian, I.K., Elliott, T., & Touret, J.L.R. (2002) Melt evolution beneath thick lithosphere: a magmatic inclusion study of La Palma, Canary Islands. Chemical Geology, 183, 169-193.

Nimis, P. (1999) Clinopyroxene geobarometry of magmatic rocks. Part 2. Structural geobarometers for basic to acidic, tholeiitic and mildly alkaline magmatic systems. Contributions to Mineralogy and Petrology, 135, 62-74.

Nimis, P., & Ulmer, P. (1998) Clinopyroxene geobarometry of magmatic rocks: Part I. An expanded structural geobarometer for anhydrous and hydrous, basic and ultrabasic systems. Contributions to Mineralogy and Petrology, 133, 122-135.

Nimis, P., & Taylor, W.R. (2000) Single clinopyroxene thermobarometry for garnet peridotites: Part I. Calibration and testing of a Cr-in-Cpx barometer and an enstatite-in-Cpx thermometer. Contributions to Mineralogy and Petrology, 139, 541-554.

Pearce, J.A., & Norry, M.J. (1979) Petrogenetic implications of Ti, Zr, Y, and Nb variations in volcanic rocks. Contributions to Mineralogy and Petrology, 69, 33-47.

Pickard, M. (2008) A Microanalytical Approach to Understanding the Origin of Cumulate Xenoliths from Mauna Kea, Hawaii. M.S. Thesis, Brigham Young University, Provo, Utah, 45 pp.

Presti, A.A. (1982) The petrology of pyroxenite xenoliths from Kaula Island, Hawaii. MS thesis, University of Hawaii, 211 pp.

Putirka K, Ryerson FJ, & Mikaelian H. (2003) New igneous thermobarometers for mafic and evolved lava compositions, based on clinopyroxene + liquid equilibria. American Mineralogist, 88, 1542-1554.

Ridolfi, F., & Renzulli, A. (2012) Calcic amphiboles in calc-alkaline and alkaline magmas: Thermobarometric and chemometric empirical equations valid up to 1,130ºC and 2.2 GPa. Contributions to Mineralogy and Petrology, 163: 877-895.

Sen, G. (1988) Petrogenesis of spinel lherzolite and pyroxenite suite xenoliths fromKoolua shield, Oahu, Hawaii: Implications for petrology of the post-eruptive lithosphere beneath Oahu. Contributions to Mineralogy and Petrology, 100, 61-91.

Sen, G., Frey, F.A., Shimizu, N., & Leeman, W.P. (1993) Evolution of the lithosphere beneath Oahu, Hawaii: rare earth element abundances in mantle xenoliths. Earth and Planetary Science Letters, 119, 53-69.

Sen, I.S., Bizimis, M., Sen, G., and Huang, S., 2011. A radiogenic Os component in the oceanic lithosphere? Constraints from Hawaiian pyroxenite xenoliths. Geochimica et Cosmochimica Acta, 75, 4899-4916.

Tartarotti, P., Susini, S., Nimis, P., & Ottolini, L. (2002) Melt migration in the upper mantle along the Romanche Fracture Zone (Equatorial Atlantic). Lithos, 63, 125-149.

Vanderkluysen, L., Mahoney, J.J., Koppers, A.A.P., Beier, C., Regelous, M., Gee, J.S., & Lonsdale, P.F. (2014) Louisville seamount chain: Petrogenetic processes and geochemical evolution of the mantle source. Geochemistry, Geophysics, Geosystems, 15, 2380-2400, doi:10.1002/2014GC005288.

Wass, S. Y. (1979) Multiple origins of clinopyroxenes in alkalic basaltic rocks. Lithos, 12, 115–132.

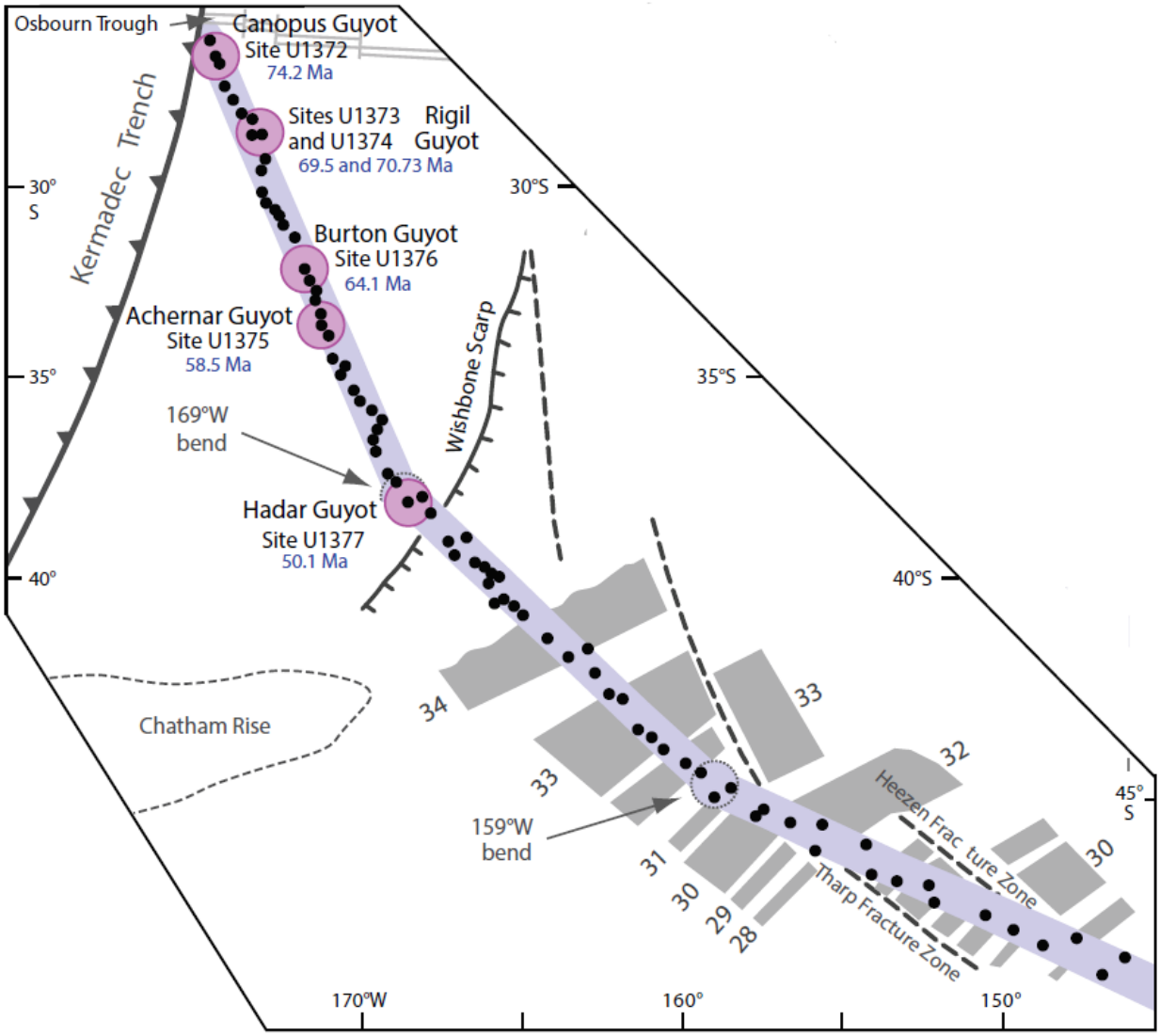

Figure 1. Generalized map of the Louisville Seamount Trail showing the location and age of the Burton Guyot drilled by IODP Expedition 330 (after Koppers et al., 2012).

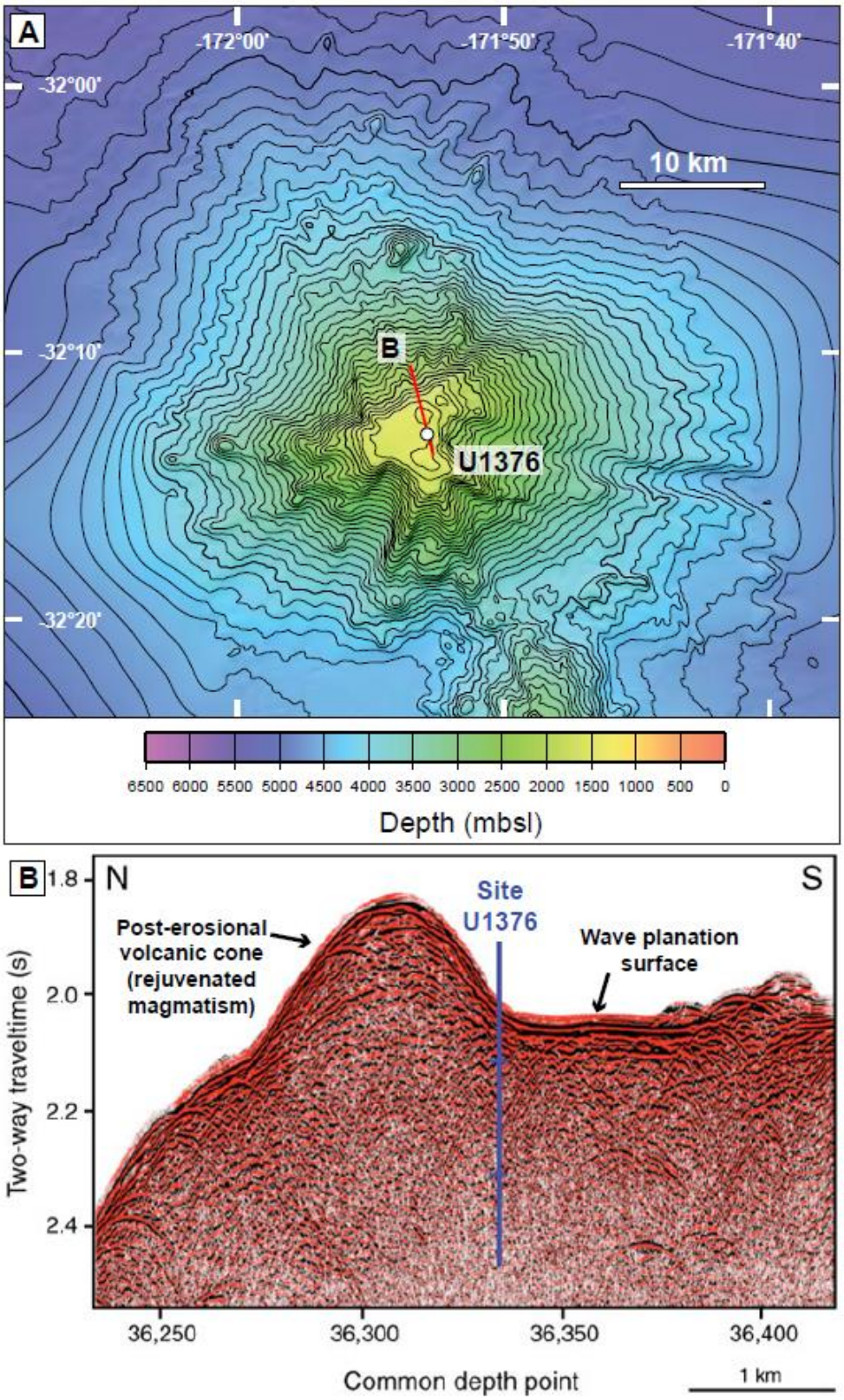

Figure 2. Bathymetric map of Burton Guyot (32.3°S Guyot) with location of IODP Site U1376, and seismic profile in red (modified from Koppers et al., 2010).

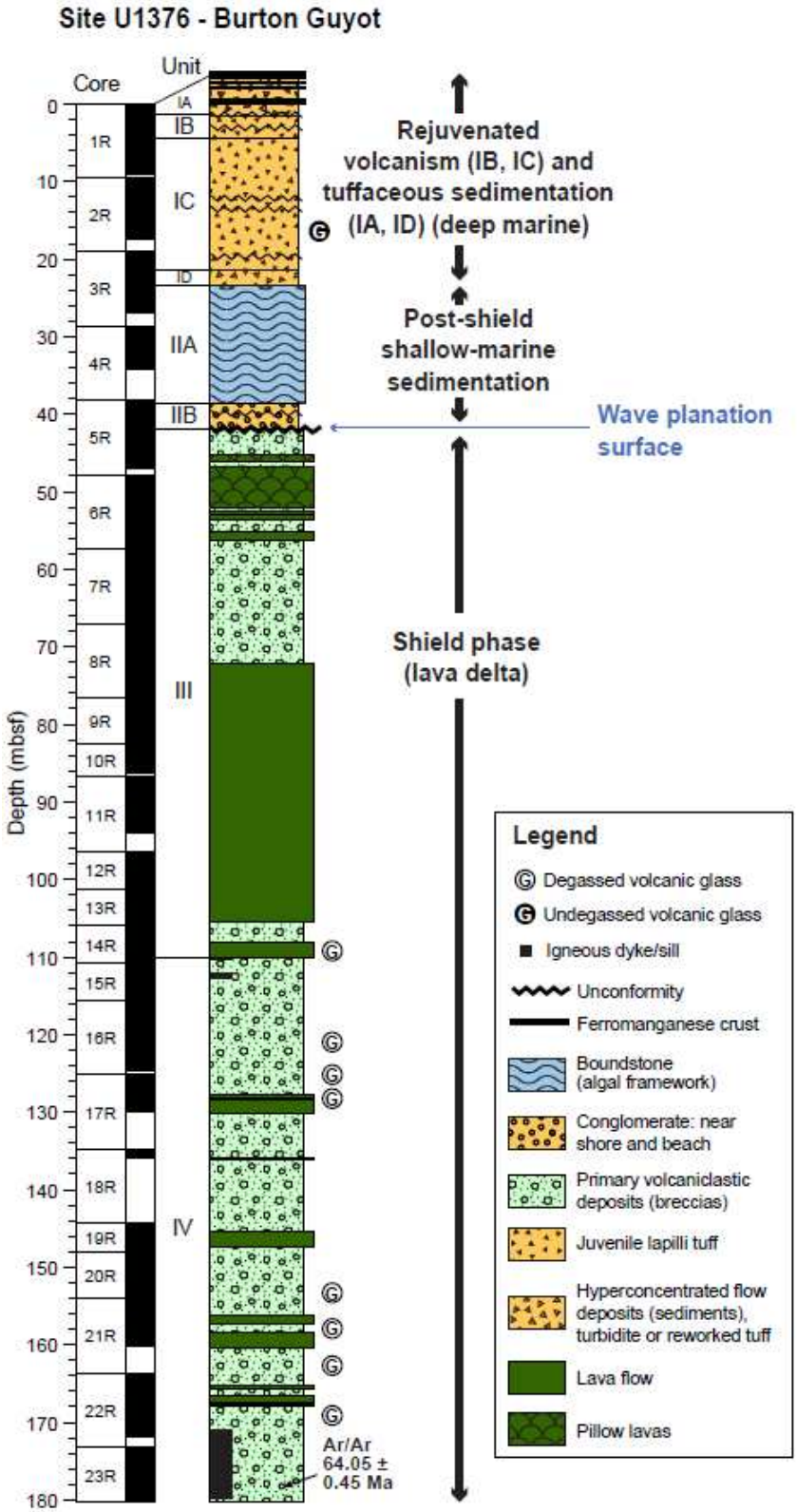

Figure 3. Stratigraphic summary of the sedimentary and volcanic sequences, Site U1376 (from Koppers et al., 2012).

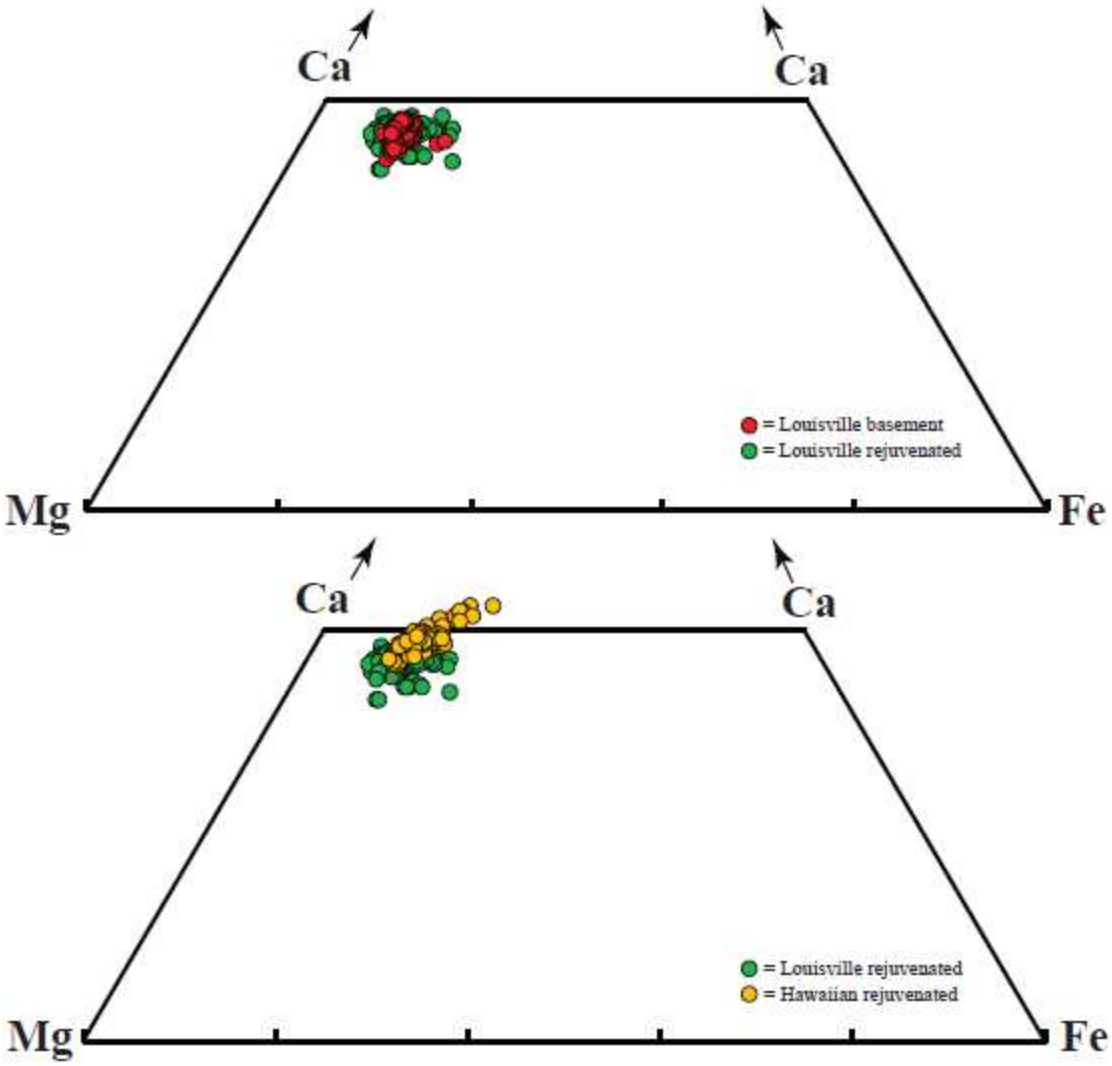

Figure 4. Pyroxene quadrilateral showing the compositions of Louisville basement and rejuvenated clinopyroxenes (4A). Hawaiian rejuvenated clinopyroxene is compared with Louisville rejuvenated clinopyroxene (4B).

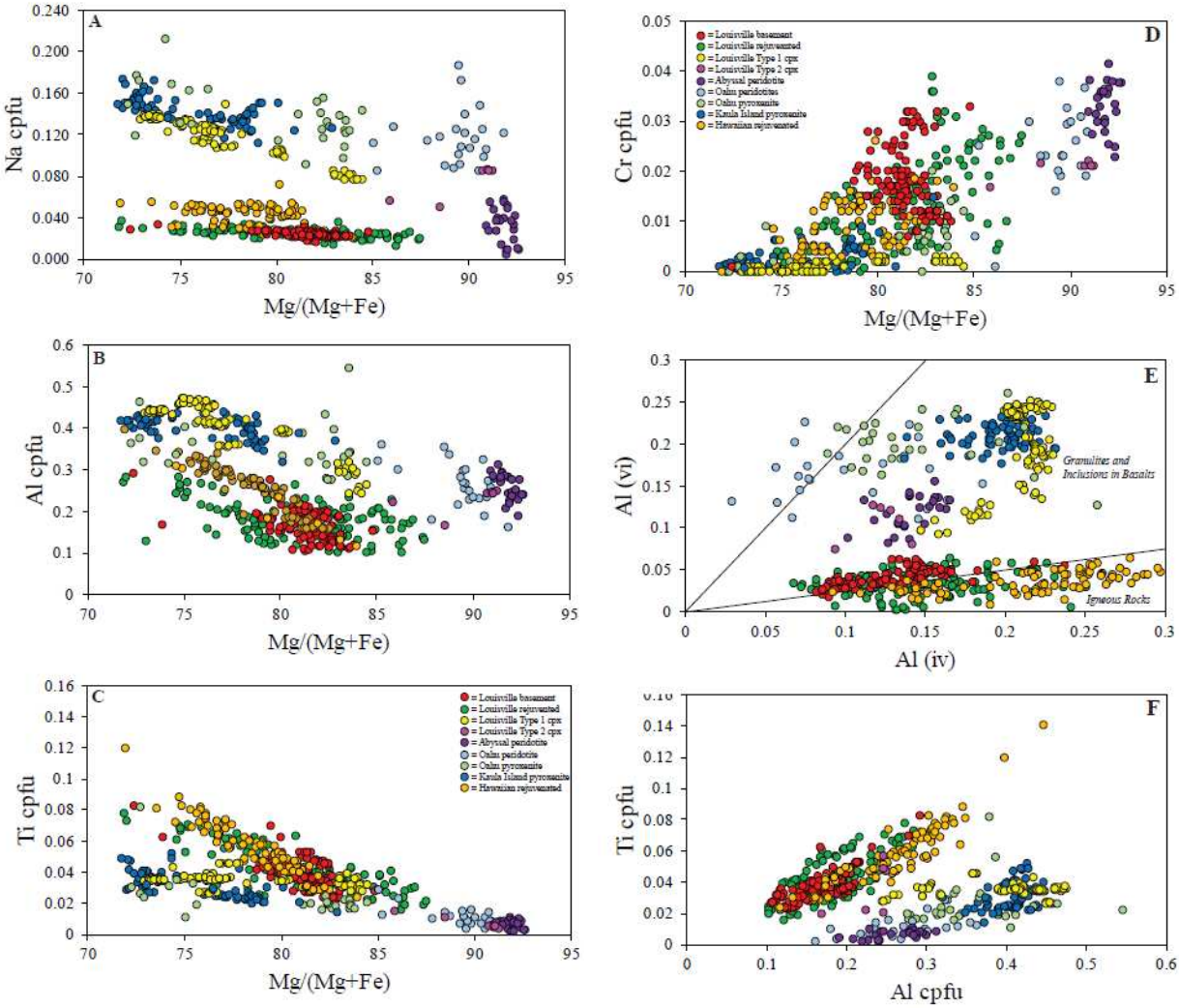

Figure 5. Na versus Mg/(Mg+Fe) (5A), Al versus Mg/(Mg+Fe) (5B), Ti versus Mg/(Mg+Fe) (5C), Cr versus Mg/(Mg+Fe) (5D), Al(vi) versus Al(iv) (5E), and Ti versus Al (5F). In each diagram, the Louisville basement and rejuvenated clinopyroxenes are identical and are similar to Hawaiian rejuvenated clinopyroxenes. Most Na-rich clinopyroxene from Louisville are similar to clinopyroxenes from Kaula Island and Salt Lake Crater, Hawaii. Other Na-rich Louisville clinopyroxenes are similar to clinopyroxene from Oahu and abyssal peridotites.

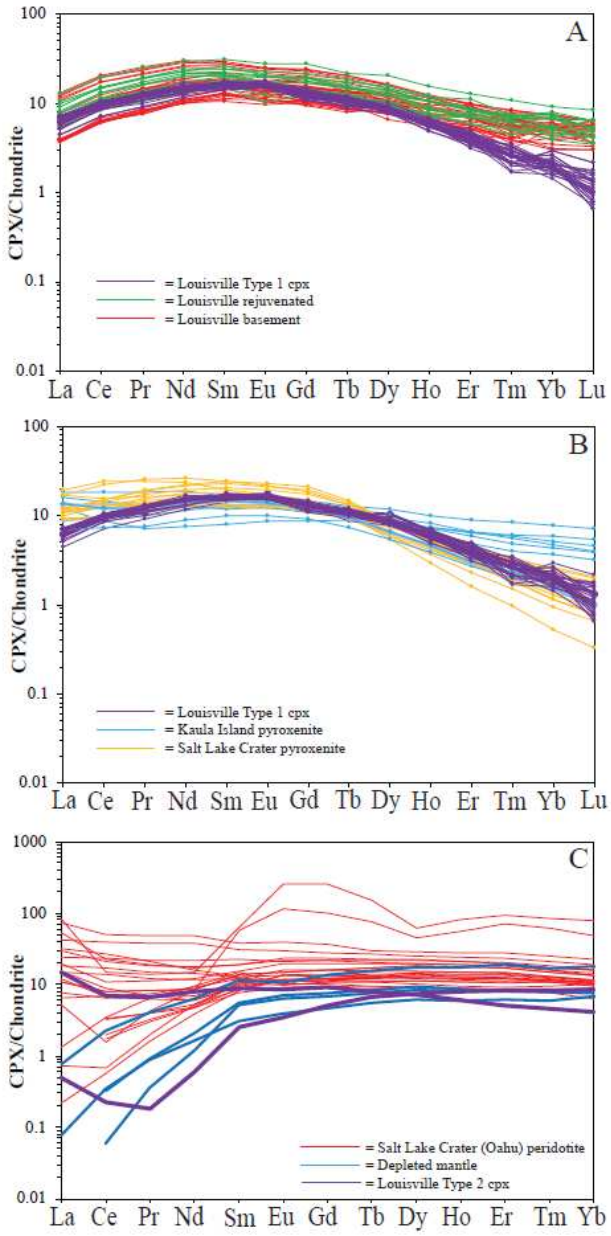

Figure 6. Chondrite-normalized REE patterns of Louisville basement and rejuvenated clinopyroxenes, compared to patterns for Na-rich Louisville grains (normalization constants from Anders and Ebihara, 1992). 6B. Comparison of Louisville Na-rich clinopyroxenes to grains from Kaula Island and Salt Lake Crater, Hawaii. 6C. Chondrite-normalized REE patterns of the smaller subset of Na-rich Burton Guyot clinopyroxene compared to clinopyroxene from Hawaiian and abyssal peridotites.

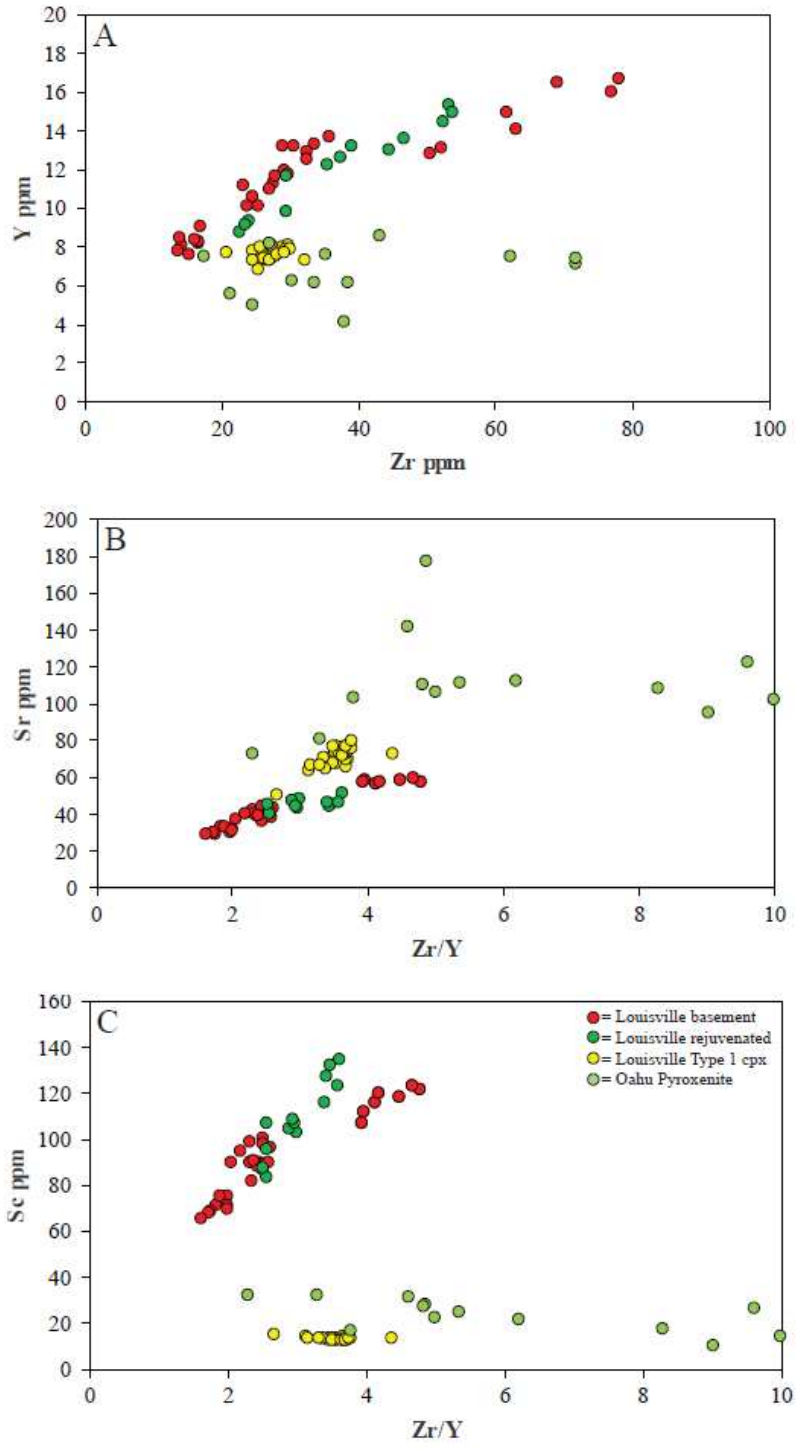

Figure 7. Y versus Zr, Sr versus Zr/Y, and Sc versus Zr/Y. Louisville rejuvenated clinopyroxenes have intermediate values, plotting along the middle of the trends defined by Louisville basement clinopyroxenes. Na-rich clinopyroxene defines its own field, especially with respect to Sc concentrations.

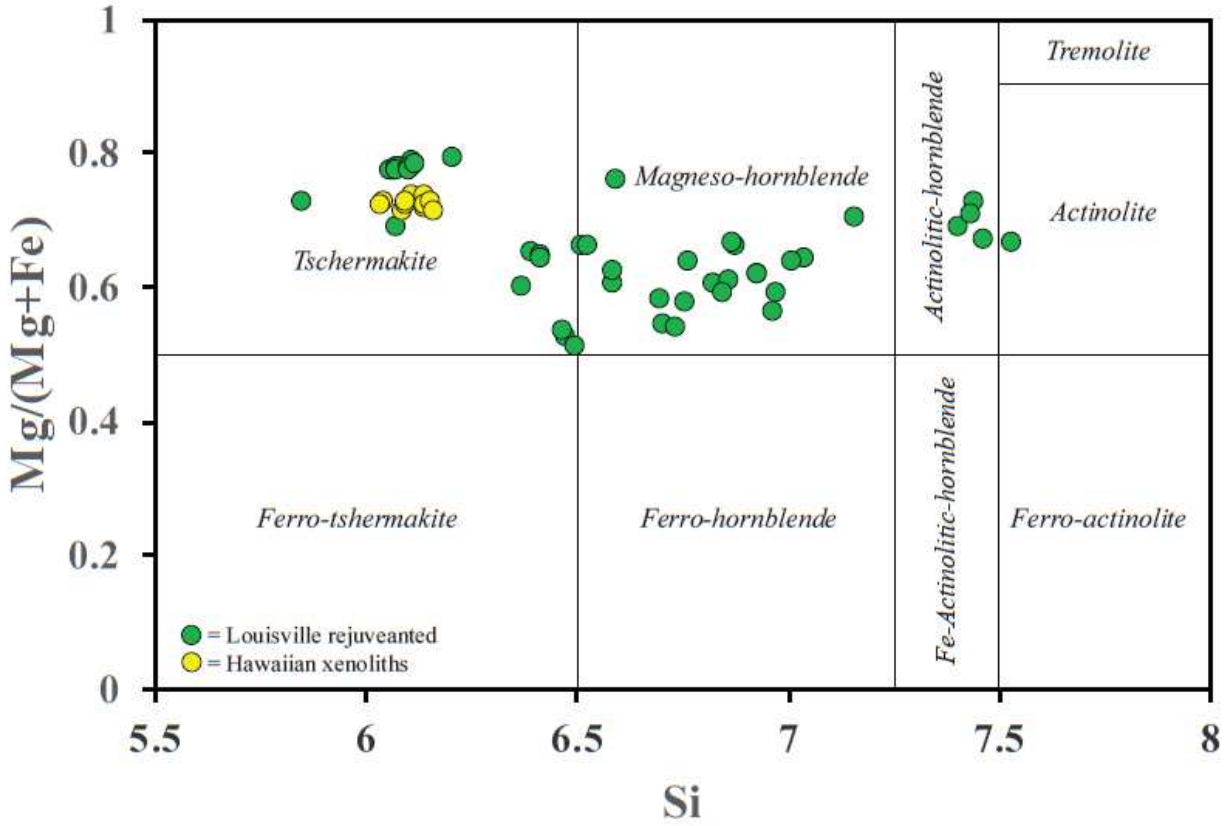

Figure 8. Mg/(Mg+Fe) versus Si (cpfu) for Burton Guyot amphiboles. Compositions range from tschermakite to actinolitic-hornblende. Amphiboles from Mauna Kea, Hawaii xenoliths are plotted for comparison (Pickard, 2008).

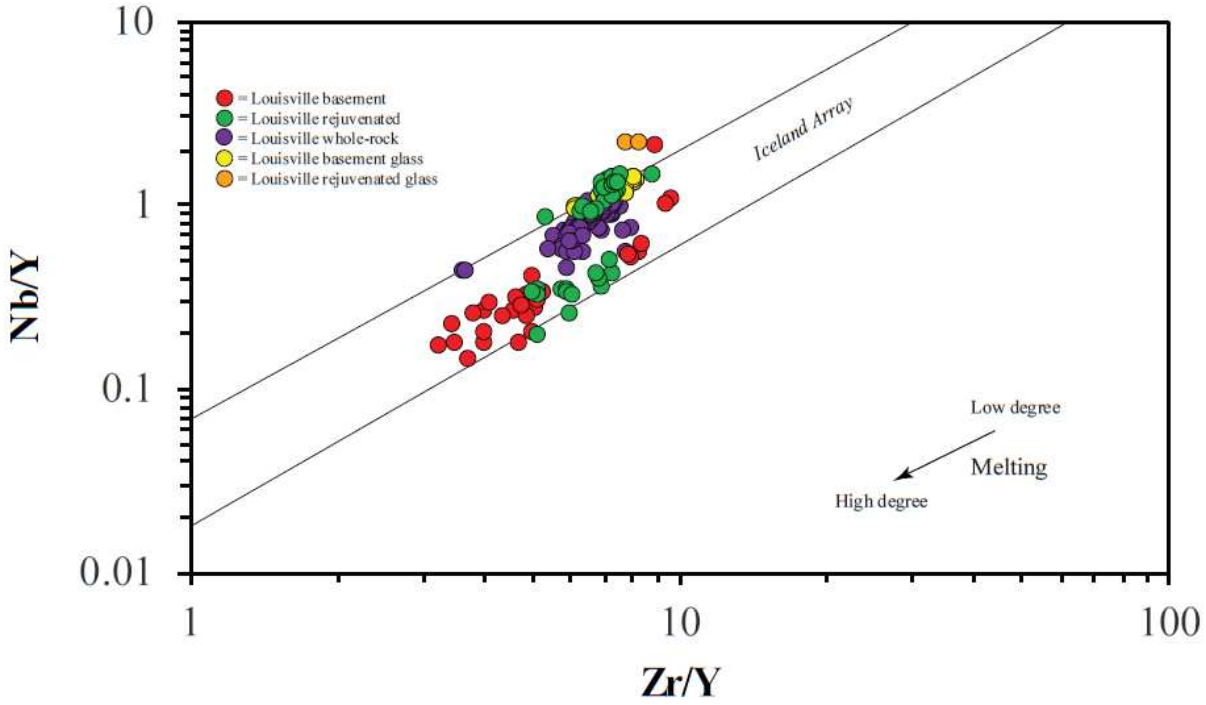

Figure 9. Nb/Y versus Zr/Y diagram (After Fitton et al., 1997). Louisville clinopyroxenes plot along the Iceland array, showing crystallization from magmas produced by variable amounts of partial melting. Liquids calculated from rejuvenated clinopyroxenes plot along the middle of the trend defined by basement clinopyroxenes, and are identical to Louisville whole-rock and glass compositions.

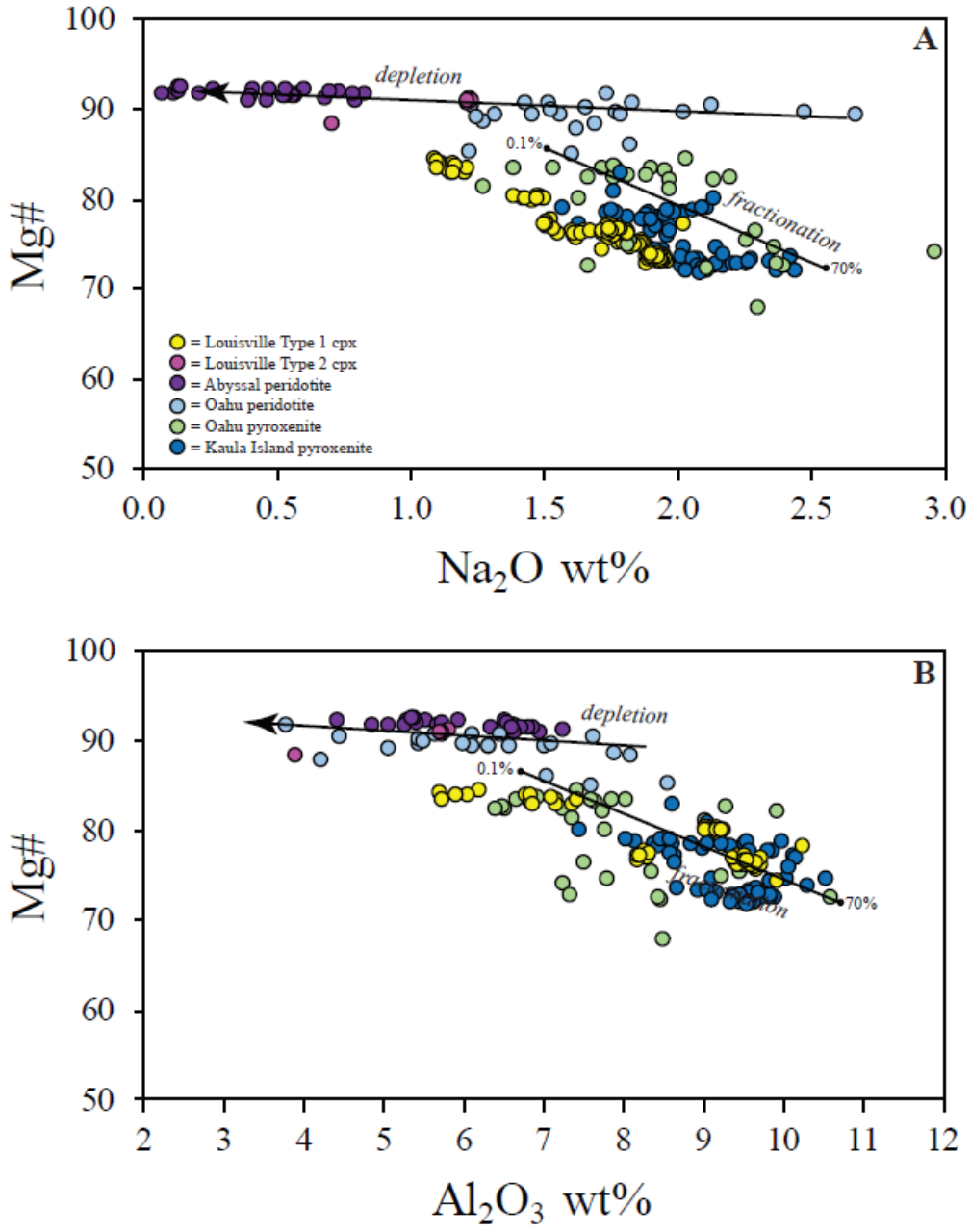

Figure 10. Mg# versus Na_2O. Al_2O_3, Zr, Sm, and Ti. Clinopyroxenes from abyssal and Salt Lake Crater pyroxenites define a trend at high Mg# over a range of Na_2O, Al_2O_3, Zr, Sm, and Ti. Increasing amounts of mantle depletion are to the left. The minor subset of Louisville Na-rich clinopyroxenes plot along this mantle xenolith trend. In contrast, clinopyroxenes from Kaula Island and Salt Lake Crater pyroxenites define fractionation trends of decreasing Mg# with increasing Na_2O, Al_2O_3, Zr, Sm, and Ti. Most of the Louisville Na-rich clinopyroxenes plot along these fractionation trends.

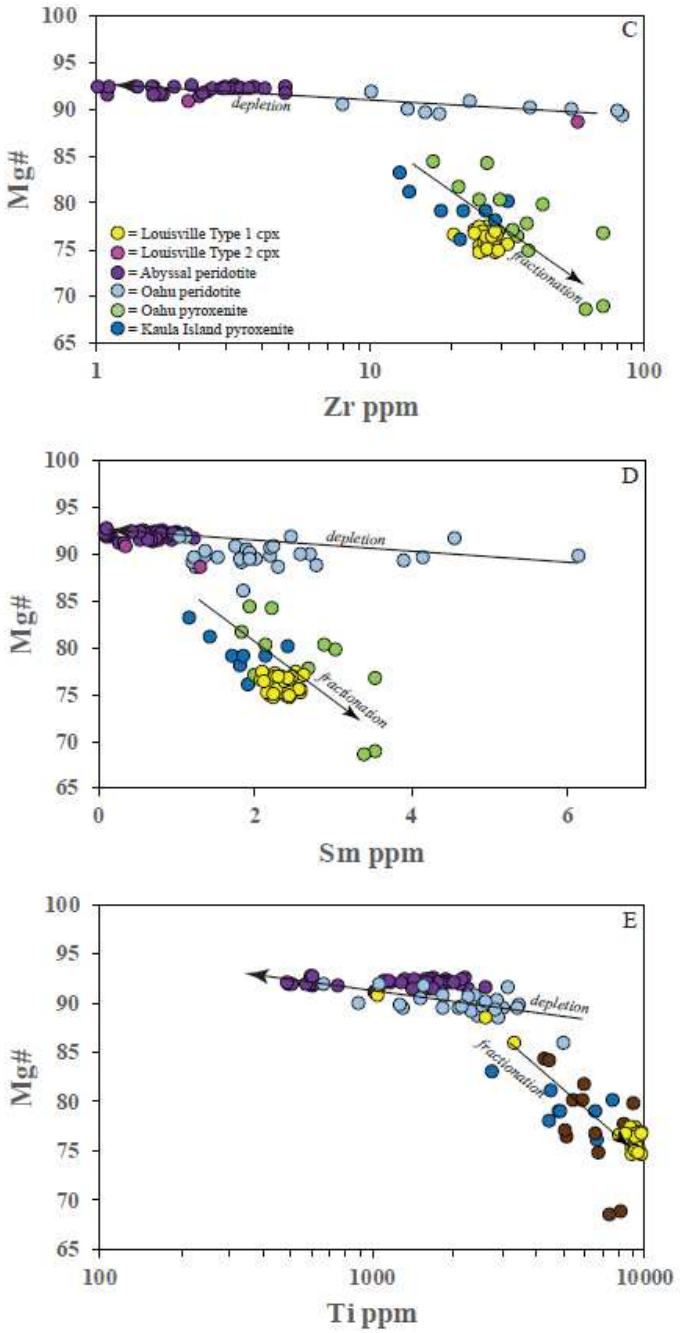

Figure 11. Pressure-temperature systematics of Louisville clinopyroxenes, compared to pyroxenites from Kaula Island (Bizimis et al., 2013) and Salt Lake Crater, Oahu (Bizimis et al., 2005). Louisville Na-rich clinopyroxene temperatures and pressures were calculated using the methods of Nimis and Taylor (2000) and Nimis and Ulmer (1998) respectively. The crystallization temperatures and pressures of phenocrystic clinopyroxenes were determined by the method of Putirka et al. (2003). The Burton Guyot amphiboles range from reaction grains at the highest P and T (Ridolfi and Renzulli, 2012) to phenocrysts reflecting increasing amounts of magma differentiation. The dry peridotite solidus is from Hirschmann (2000). The stability fields are shown schematically (after Bizimis et al., 2013).